Numerical Heat Transfer, Part A: Applications: An International Journal of Computation and Methodology
Publication details, including instructions for authors and subscription information:
http://www.tandfonline.com/loi/unht20

An Investigation of Compressible Turbulent Forced Convection by an Implicit Turbulence Model for Large Eddy Simulation

Wu-Shung Fu [a] , Chung-Gang Li [b] , Makoto Tsubokura [b] , Yun Huang [a] & J. A. Domaradzki [c]

[a] Department of Mechanical Engineering , National Chiao Tung University , Taiwan , Republic of China

[b] Complex Phenomena Unified Simulation Research Team, RIKEN, Advanced Institute for Computational Science , Kobe , Japan

[c] Department of Aerospace and Mechanical Engineering , University of Southern California , Los Angeles , California , USA

Published online: 02 Sep 2013.

To cite this article: Wu-Shung Fu , Chung-Gang Li , Makoto Tsubokura , Yun Huang & J. A. Domaradzki (2013) An Investigation of Compressible Turbulent Forced Convection by an Implicit Turbulence Model for Large Eddy Simulation, Numerical Heat Transfer, Part A: Applications: An International Journal of Computation and Methodology, 64:11, 858-878, DOI: 10.1080/10407782.2013.807663

To link to this article: http://dx.doi.org/10.1080/10407782.2013.807663

Numerical Heat Transfer, Part A, 64: 858–878, 2013

ISSN: 1040-7782 print/1521-0634 online
DOI: 10.1080/10407782.2013.807663

Taylor & Francis
Taylor & Francis Group

AN INVESTIGATION OF COMPRESSIBLE TURBULENT FORCED CONVECTION BY AN IMPLICIT TURBULENCE MODEL FOR LARGE EDDY SIMULATION

Wu-Shung Fu[1], Chung-Gang Li[2], Makoto Tsubokura[2], Yun Huang[1], and J. A. Domaradzki[3]

[1]*Department of Mechanical Engineering, National Chiao Tung University, Taiwan, Republic of China*

[2]*Complex Phenomena Unified Simulation Research Team, RIKEN, Advanced Institute for Computational Science, Kobe, Japan*

[3]*Department of Aerospace and Mechanical Engineering, University of Southern California, Los Angeles, California, USA*

An investigation of compressible turbulent forced convection in a three-dimensional channel flow is studied numerically by an implicit turbulence model for large eddy simulation (LES). Because of a high temperature difference between two walls and turbulent flow, the compressibility and viscosity of fluid should be taken into consideration simultaneously. Methods of the Roe scheme, preconditioning, and dual time stepping coordinating an implicit turbulence model for LES are used for resolving the effect of the compressibility of fluid on a low speed flow field. The magnitudes of Re_τ based on the friction velocity changing from 180 to 940, with the high temperature difference of two walls of 500 k are conducted. The results of the mean velocity profiles and turbulent intensities are in good agreement with the benchmark DNS data obtained by spectral codes from a low Reynolds number ($Re_\tau = 180$) to a high Reynolds number ($Re_\tau = 940$). Besides, the larger the Re_τ is, with the exception of acquirement of larger average Nusselt number, the more drastic variation of local instantaneous Nusselt number is observed.

1. INTRODUCTION

Recently, compressible turbulent flows at extremely low Mach numbers, such as encountered in aeroacoustics, combustion, and semiconductor manufacturing processes, etc., have attracted much attention. A method for resolving forced convection problems under a compressible turbulent flow condition is then demanded urgently.

For resolving compressible fluids in a low speed flow correctly, several related numerical methods had been proposed. For a low speed compressible flow, in an explicit

Received 3 October 2012; accepted 7 May 2013.

The authors gratefully acknowledge the support of the Natural Science Council, Taiwan, ROC under contract NSC97-2221-E-009-144, and the National Center for High-Performance Computing of Taiwan, ROC.

Address correspondence to Wu-Shung Fu, Department of Mechanical Engineering, National Chiao Tung University, 1001 Ta Hsueh Road, Hsinchu, 30056, Taiwan, Republic of China. E-mail: wsfu@mail.nctu.edu.tw

NOMENCLATURE

J	Jacobian matrix	Re_τ	Raynolds number based on friction velocity, $\left(=\frac{u_\tau \cdot (l_2/2)}{\nu}\right)$
k	thermal conductivity, W/mK	t	physical time, s
l_1, l_2, l_3	the length, height and width of channel, m	T	temperature, K
Ma	local Mach number	T_0	temperature of surroundings and cold wall, K
Nu	local Nusselt number defined in Eq. (52)	T_h	temperature of heat surface, K
$\overline{\mathrm{Nu}}$	average Nusselt number defined in Eqs. (53) and (54)	u_1, u_2, u_3	velocities in x_1, x_2, and x_3 directions, m/s
P	pressure, Pa	u_τ	friction velocity, m/s
P_0	surrounding pressure, Pa	x_1, x_2, x_3	cartesian coordinates, m
Pr	Prandtl number	ρ	density, $\mathrm{kg/m^3}$
R	gas constant, J/kg/K	ρ_0	surrounding density, $\mathrm{kg/m^3}$
Re	Raynolds number based on average main flow velocity, $\left(=\frac{\bar{u}_1 \cdot (l_2/2)}{\nu}\right)$	μ	viscosity, $\mathrm{N \cdot s/m^2}$
		γ	specific heat ratio
		τ	artificial times, s

numerical method, the limitation of CFL condition would cause an inefficient calculation due to the extremely small time step. In this article, an implicit method is used and then a magnitude of the time step can be slightly larger than that limited by CFL condition and used in an explicit method. In an implicit numerical method, the stiff situation causes an inefficiency of calculation to occur easily. For overcoming these defects mentioned above, Briley et al. [1] used a preconditioning method to improve the efficiency of calculation for a low Mach number flow, and adopted the implicit numerical method to resolve the convergent problem of the Navier-Stokes equation. Turkel [2] developed and applied a preconditioning matrix into problems of compressible and incompressible flows. Choi and Merkel [3] investigated convergent problems induced by the stiff situation and factorization error when an implicit numerical method was used to solve inviscid flow under a low Mach number flow. Moreover, the convergent problem of the Mach number of 0.05 was successfully resolved by using the precondition matrix. Afterward Choi and Merkel [4] proposed an adaptable preconditioning matrix to solve convergent problems of a viscous flow under a low Mach number situation. Roe [5] developed average variables method for a compressible flow to solve discontinuous phenomenon occurring at a cell interface. This method has been widely used in solving compressible flows recently. Weiss and Smith [6] extended the research of Choi and Merkel [4] and applied the Roe scheme mentioned above with the preconditioning method into the solution method of three-dimensional Navier-Stokes equations, and added a dual time stepping to resolve transient states of a low Mach number flow. Thornber and Drikakis [7] modified the Roe scheme to reduce the excess dissipation of kinetic energy in Godunov-type methods at low Mach numbers. It had been shown that this modification for Kelvin–Helmholtz instability problems could work efficiently at $\mathrm{Ma} = 0.0002$. Dellacherie [8] investigated the inaccurate phenomena when using the Godunov type schemes applied at low Mach numbers and proposed a new modification on the Roe–Turkel and the AUSM+-up schemes. This new modification showed that it could obtain stable and accurate numerical results at a low Mach number on quadrangular and triangular meshes.

However, due to the complicated numerical scheme of the compressible turbulence in low speed regions, there is comparatively minimal literature adopting the methods of LES and preconditioning simultaneously. Lessani et al. [9] applied the preconditioning method with the multigrid skill into the LES method to simulate a channel and cavity flows. The results showed that the convergence speed is increased 4–7 times compared with an explicit method. Xiaofeng et al. [10] used the finite volume and LES methods to calculate a pipe flow. The results compared with the results of experimental and DNS methods showed good agreement. Alkishriwi et al. [11] calculated a channel and a circular flow by the LES method matching the methods of preconditioning and multigrid under different Mach numbers and time intervals. This synthetic method had wonderful efficiency, and improved the calculating convergence of compressible problems of low Mach numbers remarkably. The convergent speed of this method was quicker than that of the method of the fifth order Runge-Kutta about 4–60 times. In the referenced literature, although the combinations of methods of preconditioning and LES have been implemented successfully, the Reynolds numbers are still not high enough for practical applications. Also, there is not much discussion about the effects of the turbulence model on low speed compressible flows.

In order to broaden the practical applications widely, the turbulence model which is easily programmable at higher Reynolds numbers, is needed urgently. In a review article of Domaradzki and Adams [12] a concept was proposed with appropriate neglect of the nonlinear terms which were under-resolved, the application of deconvolution in the LES was the same with solving the truncated Navier-Stokes (TNS) equations for the de-filtered velocity. By this concept, the LES equations could be enclosed by the results of the subgrid scale (SGS) terms computed explicitly by the TNS equations. This method, named estimation model, could predict turbulent flows accurately. However, the original estimation model was not efficient enough due to the necessity of computing the LES and TNS equations simultaneously. In order to overcome the low efficiency, Domaradzki et al. [13] simplified the estimation model by dispensing with the LES equations entirely in favor of only using the TNS equations. Such a simplification came from the observation that large scales of the flow were already contained in the TNS velocity on the fine meshes so that the LES equations could be eliminated. Besides, because of the under-resolved DNS, the accumulation of the energy in small scales caused the incorrectness of the dynamics; the secondary filter was used by a periodic filtering to remove this kind of energy. Stolz and Adam [14] computed the SGS directly from the defiltered velocity filtered by using the approximate deconvolution model (ADM). Fureby and Grinstein [15] proposed a new method named the monotonically integrated large eddy simulation (MILES) to simulate the free shear flows. By using the high-resolution monotone algorithms with the limiting flux, the phenomena in the subgrid scale could be modeled by numerical truncation error. However, Domaradzki and Radhakrishnan [16] indicated that MILES was not suitable for the decaying high Reynolds number turbulence. From above, the fact was recognized that no matter which turbulence model is adopted, all would try to dissipate the unphysical energy which was under-resolved and accumulated in small scales.

Therefore, the aim of this study is to propose a new implicit turbulence model of LES to investigate heat transfer mechanisms of a three-dimensional channel flow under fully developed compressible turbulent flows. In this new turbulence model,

the Roe upwinding dissipation term acts as an implicit turbulence model for LES. Besides, in order to capture the turbulence structure as small as possible, the grid distribution near the wall is arranged densely by a curvilinear transformation method. With the excellent advantages of easy implementation in the curvilinear coordinate, this model is used to study heat transfer mechanisms of the fully developed compressible turbulent channel flows, which vary from a low Reynolds number ($\mathrm{Re}_\tau = 180$) to a high Reynolds number ($\mathrm{Re}_\tau = 940$). The results show that a cluster of big lumps made of isothermal surface of fluids are observed under a situation of small magnitude of Re_τ. Accompanying the increment of Re_τ, the lumps are gradually torn into an aggregation of small fragments of isothermal surface due to the drastic fluctuating velocities existing in a large magnitude of Re_τ. The larger the Re_τ is, the larger the averaged Nusselt number is. Also, the variation of the local instantaneous Nusselt number under a large magnitude of Re_τ is much more drastic than that under a small magnitude of Re_τ. Finally, for the purpose of practical applications, the average Nusselt number obtained from the numerical results can be expressed as a function of the Reynolds numbers, the trend of which is similar to the experimental data.

2. PHYSICAL MODEL

A three-dimensional situation of a fully developed compressible turbulent forced convection in a channel flow is investigated, and the physical model is shown in Figure 1. The streamwise, vertical, and spanwise directions are x_1, x_2, and x_3, respectively, and the corresponding velocities are u_1, u_2, and u_3, respectively. The length, height, and width are l_1, l_2, and l_3, respectively. Fluids which possess mean velocity $\bar{u}_1$ and temperature T_0 flow into parallel plates. The temperatures of the bottom and upper surfaces are T_h and T_0, respectively. In the spanwise direction, a periodical condition is adopted on the both sides. In the streamwise direction, fully developed conditions of flowing and thermal fields are used at the end of computation processes. The LES with the implicit turbulence model is adopted to solve heat transfer mechanisms of the above situation, and then the Navier-Stokes equations have no necessity to be modeled.

For facilitating the analysis, the following assumptions are made.

1. The fluid is an ideal gas and follows the state of equation.
2. The effect of gravity is neglected due to the magnitude of $\mathrm{Gr}/\mathrm{Re}^2$ is very small.

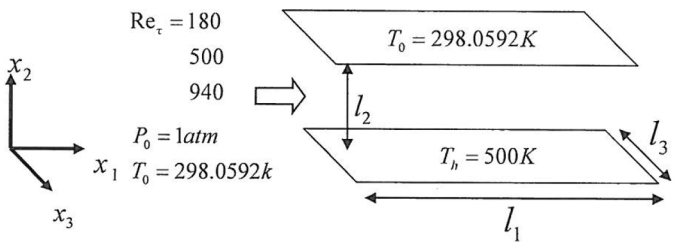

Figure 1. Physical model.

The governing equations are expressed as Eq. (1).

$$\frac{\partial U}{\partial t}+\frac{\partial F_1}{\partial x_1}+\frac{\partial F_2}{\partial x_2}+\frac{\partial F_3}{\partial x_3}=0 \tag{1}$$

The quantities included in U and F_i are separately shown in the following equations.

$$U=\begin{pmatrix}\rho\\ \rho u_1\\ \rho u_2\\ \rho u_3\\ \rho e\end{pmatrix} \tag{2}$$

and

$$F_i=\begin{pmatrix}\rho u_i\\ \rho u_i u_1+P\delta_{i1}-\mu A_{i1}\\ \rho u_i u_2+P\delta_{i2}-\mu A_{i2}\\ \rho u_i u_3+P\delta_{i3}-\mu A_{i3}\\ (\rho e+P)u_i-\mu A_{ij}u_j-k\frac{\partial T}{\partial x_i}\end{pmatrix}, \forall i=1,2,3 \tag{3}$$

where $A_{ij}=\frac{\partial u_j}{\partial x_i}+\frac{\partial u_i}{\partial x_j}-\frac{2}{3}(\nabla\bullet u)\delta_{ij}$ and e is the internal energy. The state equation of ideal gas is written by Eq. (4)

$$P=\rho RT \tag{4}$$

The viscosity and thermal conductivity of the fluid are based upon Sutherland's law and are shown as follows.

$$\mu(T)=\mu_0\left(\frac{T}{T_0}\right)^{\frac{2}{3}}\frac{T_0+110}{T+110} \tag{5}$$

$$k(T)=\frac{\mu(T)\gamma R}{(\gamma-1)\,\mathrm{Pr}} \tag{6}$$

Where, $\rho_0=1.1842\,\mathrm{kg/m^3}$, $\mu_0=1.85\times10^{-5}\,\mathrm{N\cdot s/m^2}$, $\mathrm{T}_0=298.0592\,\mathrm{K}$, $\gamma=1.4$, $\mathrm{R}=287\,\mathrm{J/kg/K}$, and $\mathrm{Pr}=0.72$.

3. NUMERICAL METHOD

In order to accurately obtain compressible turbulent forced convection phenomena by the LES method, a high order differentiation for the derivative term of MUSCL scheme is necessary. Besides, for satisfying the characteristics of three-dimensional eddy motions of the turbulent flow, based on Tankitul and Domaradzki [17], the half height of the channel is regarded as a characteristic length, and the length and width of the channel shown in Figure 1 being 2.5π and 0.5π times the magnitude of the characteristic length are adopted in the streamwise and spanwise directions, respectively.

Except usage of Roe and preconditioning methods, two effective methods are used to avoid the occurrence of inefficiency and inaccuracy in computing processes. One is the method of transformation of three-dimensional curvilinear coordinates (ξ, η, ζ) to be used; then, near the wall the smallest eddy scale of turbulent flow can be captured. A dual time stepping process is the other way to improve the efficiency of convergence. The original governing equation (Eq. 1) is then transformed into the following equation.

$$\Gamma\frac{\partial\overline{U}_p}{\partial\tau}+\frac{\partial\overline{U}}{\partial t}+\frac{\partial\overline{F}_1}{\partial\xi}+\frac{\partial\overline{F}_2}{\partial\eta}+\frac{\partial\overline{F}_3}{\partial\zeta}=0 \tag{7}$$

where Γ is the preconditioning matrix derived by Weiss and Smith [6], and $\overline{U}_p$ is the primitive form $[P, u_1, u_2, u_3, T]/J$ in which J is the Jacobian matrix. τ and t are the artificial and physical times, respectively, and $\overline{U}$ is the conservative form of $(\rho, \rho u_1, \rho u_2, \rho u_3, \rho e)/J$. The preconditioning parameter β according to Weiss and Smith [6] is chosen as $\beta = max(min(M^2, 1.0), \beta_{min})$, where M is the local Mach number and $\beta_{\min} \approx 3M_\infty^2$. M_∞ is the approaching Mach number.

To discretize Eq. (7), Eq. (8) is obtained. The terms of $\frac{\partial\overline{U}_p}{\partial\tau}$ and $\frac{\partial\overline{U}}{\partial t}$ are differentiated by the first order forward difference and the second order backward difference, respectively, and the terms of $\frac{\partial\overline{F}_1}{\partial\xi}$, $\frac{\partial\overline{F}_2}{\partial\eta}$, and $\frac{\partial\overline{F}_3}{\partial\zeta}$ are differentiated by the central difference.

$$\begin{aligned}\Gamma&\frac{\overline{U}_p^{k+1}-\overline{U}_p^{k}}{\Delta\tau}+\frac{3\overline{U}^{k+1}-4\overline{U}^{n}+\overline{U}^{n-1}}{2\Delta t}\\&+\frac{1}{\Delta\xi}\left(\overline{F}_{1_{i+\frac{1}{2},j,k}}^{k+1}-\overline{F}_{1_{i-\frac{1}{2},j,k}}^{k+1}\right)+\frac{1}{\Delta\eta}\left(\overline{F}_{2_{i,j+\frac{1}{2},k}}^{k+1}-\overline{F}_{2_{i,j-\frac{1}{2},k}}^{k+1}\right)\\&+\frac{1}{\Delta\zeta}\left(\overline{F}_{3_{i,j,k+\frac{1}{2}}}^{k+1}-\overline{F}_{3_{i,j,k-\frac{1}{2}}}^{k+1}\right)=0\end{aligned} \tag{8}$$

In which superscripts of k and n indicate the iteration numbers of artificial time and proceeding step of real time, respectively. When the term of artificial time $\frac{\partial\overline{U}_p}{\partial\tau}$ is convergent to $\varepsilon(=10^{-2})$, Eq. (8) is automatically transferred into the Navier-Stokes equation and the values at the iteration number of $(k+1)$ of the artificial time in Eq. (8) substantially become the values at the proceeding step of $(n+1)$ of the real time.

Afterward, the terms of $\overline{U}^{k+1}$ and $\overline{F}_i^{k+1}$ in Eq. (8) are necessary to be linearized and expressed as follows, respectively.

$$\overline{U}^{k+1}=\overline{U}^{k}+M\Delta\overline{U}_p \tag{9}$$

Where $M=\frac{\partial\overline{U}}{\partial\overline{U}_p}$ and $\Delta\overline{U}_p=\overline{U}_p^{k+1}-\overline{U}_p^{k}$

$$\overline{F}_1^{K+1}=\overline{F}_1^{K}+A_p\Delta\overline{U}_p \tag{10}$$

Where $A_p=\frac{\partial\overline{F}_1^{k}}{\partial\overline{U}_p}$ is the flux Jacobian and the same method for $B_p=\frac{\partial\overline{F}_2^{k}}{\partial\overline{U}_p}$ and $C_p=\frac{\partial\overline{F}_3^{k}}{\partial\overline{U}_p}$ is used in linearization of $\overline{F}_2^{K+1}$ and $\overline{F}_3^{K+1}$, respectively.

To substitute Eqs. (9) and (10) into Eq. (11), the following equation is obtained.

$$\Gamma\frac{\Delta\overline{U}_p}{\Delta\tau}+\frac{3(\overline{U}^k+M\Delta\overline{U}_p)-4\overline{U}^n+\overline{U}^{n-1}}{2\Delta t}+\delta_\xi\left(\overline{F}_1^k+A_p\Delta\overline{U}_p\right)+\delta_\eta\left(\overline{F}_2^k+B_p\Delta\overline{U}_p\right)+\delta_\zeta\left(\overline{F}_3^k+C_p\Delta\overline{U}_p\right)=0 \tag{11}$$

where δ_ξ, δ_η, and δ_ς are central-difference operators.

Equation (11) can be rearranged as the following form.

$$\left[\Gamma\frac{I}{\Delta\tau}+M\frac{3}{2\Delta t}+\left(\delta_\xi A_p+\delta_\eta B_p+\delta_\zeta C_p\right)\right]\Delta U_p=R^k \tag{12}$$

Where $R^k=-\left(\frac{3\overline{U}^k-4\overline{U}^n+\overline{U}^{n-1}}{2\Delta t}\right)-\left(\delta_\xi\overline{F}_1^k+\delta_\eta\overline{F}_2^k+\delta_\zeta\overline{F}_3^k\right)$, I is the unit matrix.

To divide the Γ in both sides, the following equation is obtained.

$$\left[\frac{I}{\Delta\tau}+\Gamma^{-1}M\frac{3}{2\Delta t}+\Gamma^{-1}\left(\delta_\xi A_p^k+\delta_\eta B_p^k+\delta_\zeta C_p^k\right)\right]\Delta U_p=\Gamma^{-1}R^k \tag{13}$$

The solver of Eq. (14) is the LUSGS implicit method originally proposed by Yoon and Jameson [18]. However, the original method is not suitable for Eq. (13) due to a lack of the preconditioning matrix. In order to improve the LUSGS method to solve Eq. (13), the following complicated procedures are used.

$$\begin{aligned}\tilde{A}_p&=\Gamma^{-1}A_p^k\\ \tilde{B}_p&=\Gamma^{-1}B_p^k\\ \tilde{C}_p&=\Gamma^{-1}C_p^k\end{aligned} \tag{14}$$

There $\tilde{A}_p,\tilde{B}_p,$ and $\tilde{C}_p$ are divided into two parts, respectively.

$$\begin{aligned}\tilde{A}_p&=\tilde{A}_p^+ +\tilde{A}_p^-\\ \tilde{B}_p&=\tilde{B}_p^+ +\tilde{B}_p^-\\ \tilde{C}_p&=\tilde{C}_p^+ +\tilde{C}_p^-\end{aligned} \tag{15}$$

where

$$\begin{aligned}\tilde{A}_p^\pm&=\frac{1}{2}(\tilde{A}_p\pm|\lambda_{\tilde{A}}|I)\\ \tilde{B}_p^\pm&=\frac{1}{2}(\tilde{B}_p\pm|\lambda_{\tilde{B}}|I)\\ \tilde{C}_p^\pm&=\frac{1}{2}(\tilde{C}_p\pm|\lambda_{\tilde{C}}|I)\end{aligned} \tag{16}$$

$\lambda_{\tilde{A}},\lambda_{\tilde{B}},$ and $\lambda_{\tilde{C}}$ are the largest eigenvalues of $\tilde{A}_p,\tilde{B}_p,$ and $\tilde{C}_p$, respectively.

To substitute Eqs. (14) and (16) into Eq. (13), the following equation is obtained.

$$\left[\frac{I}{\Delta\tau}+\Gamma^{-1}M\frac{3}{2\Delta t}+\delta_\xi\left(\tilde{A}_p^+ + \tilde{A}_p^-\right)+\delta_\eta\left(\tilde{B}_p^+ + \tilde{B}_p^-\right) + \delta_\zeta\left(\tilde{C}_p^+ + \tilde{C}_p^-\right)\right]\Delta\overline{U}_p = \Gamma^{-1}R^k \tag{17}$$

The convective terms of $\delta_\xi\left(\tilde{A}_p^+ + \tilde{A}_p^-\right)$ can be solved by a high order scheme as the following equation.

$$\delta_\xi(\tilde{A}_p^+ + \tilde{A}_p^-) = \delta_\xi^-\tilde{A}_p^+ + \delta_\xi^+\tilde{A}_p^- = \frac{\tilde{A}_{p,i}^+ - \tilde{A}_{p,i-1}^+}{\Delta\xi} + \frac{\tilde{A}_{p,i+1}^- - \tilde{A}_{p,i}^-}{\Delta\xi} \tag{18}$$

Where the backward difference approximation δ_ξ^- is adopted for $\tilde{A}_p^+$, and the forward difference δ_ξ^+ approximation is adopted for $\tilde{A}_p^-$.

To substitute Eq. (18) into Eq. (17), the following equation can be derived.

$$\left[\frac{I}{\Delta\tau}+\Gamma^{-1}M\frac{3}{2\Delta t}+\frac{\tilde{A}_{p,i}^+ - \tilde{A}_{p,i-1}^+}{\Delta\xi}+\frac{\tilde{A}_{p,i+1}^- - \tilde{A}_{p,i}^-}{\Delta\xi} + \frac{\tilde{B}_{p,j}^+ - \tilde{B}_{p,j-1}^+}{\Delta\eta}+\frac{\tilde{B}_{p,j+1}^- - \tilde{B}_{p,j}^-}{\Delta\eta} + \frac{\tilde{C}_{p,k}^+ - \tilde{C}_{p,k-1}^+}{\Delta\zeta}+\frac{\tilde{C}_{p,k+1}^- - \tilde{C}_{p,k}^-}{\Delta\zeta}\right]\Delta\overline{U}_p = \Gamma^{-1}R^k \tag{19}$$

Eq. (19) can be arranged as the following equation.

$$(L+D+U)\Delta\overline{U}_p = \Gamma^{-1}R^k \tag{20}$$

Where

$$L = -\left[\frac{1}{\Delta\xi}(\tilde{A}_p^+)_{i-1,j,k}+\frac{1}{\Delta\eta}(\tilde{B}_p^+)_{i,j-1,k}+\frac{1}{\Delta\zeta}(\tilde{C}_p^+)_{i,j,k-1}\right] \tag{21}$$

$$D = \frac{I}{\Delta\tau}+\Gamma^{-1}M\frac{3}{2\Delta t}+\left[\frac{1}{\Delta\xi}((\tilde{A}_p^+)_{i,j,k}-(\tilde{A}_p^-)_{i,j,k}) + \frac{1}{\Delta\eta}((\tilde{B}_p^+)_{i,j,k}-(\tilde{B}_p^-)_{i,j,k})+\frac{1}{\Delta\zeta}((\tilde{C}_p^+)_{i,j,k}-(\tilde{C}_p^-)_{i,j,k})\right] \tag{22}$$

$$U = \left[\frac{1}{\Delta\xi}(\tilde{A}_p^-)_{i+1,j,k}+\frac{1}{\Delta\eta}(\tilde{B}_p^-)_{i,j+1,k}+\frac{1}{\Delta\zeta}(\tilde{C}_p^-)_{i,j,k+1}\right] \tag{23}$$

As for the computation of $R^k = -\left(\frac{3\overline{U}^k - 4\overline{U}^n + \overline{U}^{n-1}}{2\Delta t}\right) - \left(\delta_\xi \overline{F}_1^k + \delta_\eta \overline{F}_2^k + \delta_\varsigma \overline{F}_3^k\right)$ on the right-hand side (RHS) of Eq. (13), the terms of F_i in Eq. (4) based on the Cartesian coordinate can be divided into two parts. One is the inviscid term $F_{inviscid}$.

$$F_{inviscid} = \begin{pmatrix} \rho u_i \\ \rho u_i u_1 + P\delta_{i1} \\ \rho u_i u_2 + P\delta_{i2} \\ \rho u_i u_3 + P\delta_{i3} \\ (\rho e + P)u_i \end{pmatrix} \tag{24}$$

The other is viscous term $F_{viscous}$.

$$F_{viscous} = -\begin{pmatrix} 0 \\ \mu A_{i1} \\ \mu A_{i2} \\ \mu A_{i3} \\ \mu A_{ij} u_j + \lambda \frac{\partial T}{\partial x_i} \end{pmatrix} \tag{25}$$

The Roe upwind difference scheme [5] is employed in discretion of the term of $F_{inviscid}$ at the cells interface $\left(i + \frac{1}{2}\right)$, and is expressed as follows at a low Mach number situation.

$$F_{inviscid,i+\frac{1}{2}} = \frac{1}{2}(F_R + F_L) - \frac{1}{2}\varepsilon\left\{\left|\Gamma^{-1}A_p\right|\Delta U_P\right\} \tag{26}$$

In the Roe scheme [5], the Roe upwinding dissipation term $\frac{1}{2}\varepsilon\left\{\left|\Gamma^{-1}A_p\right|\Delta U_P\right\}$ is used to tackle with the discontinuous problem, so ε is always set to 1 to stabilize the numerical scheme. The Roe upwinding dissipation term might remove some turbulent kinetic energy, which is composed of jumps of properties of work fluids. In terms of numerical simulation, an appropriate magnitude of ε could make the Roe upwinding dissipation term be an implicit turbulence model. According to Tong [19] and tests of this study shown in the next section, the optimal value of ε for turbulence simulation is 0.1.

The fifth order MUSCL scheme proposed by Abalakin et al. [20] is used to compute Eq. (26), and solution procedures of ΔU_P are indicated as follows.

$$\Delta U_P = u^L_{i+1/2} - u^R_{i+1/2} \tag{27}$$

$$u^L_{i+1/2} = u_i + 1/2\ \Delta u^L_{i+1/2} \tag{28}$$

$$u^R_{i+1/2} = u_i - 1/2\ \Delta u^R_{i+1/2} \tag{29}$$

$$\begin{aligned} \Delta u^L_{i+1/2} = {} & (1-\beta)(u_{i+1} - u_i) + \beta(u_i - u_{i-1}) \\ & + \theta^c(-u_{i-1} + 3u_i - 3u_{i+1} + u_{i+2}) \\ & + \theta^d(-u_{i-2} + 3u_{i-1} - 3u_i + u_{i+1}) \end{aligned} \tag{30}$$

$$\Delta u^R_{i+1/2} = (1-\beta)(u_{i+1}-u_i) + \beta(u_{i+2}-u_{i+1}) + \theta^c(-u_{i-1}+3u_i-3u_{i+1}+u_{i+2}) + \theta^d(-u_i+3u_{i+1}-3u_{i+2}+u_{i+3}) \quad (31)$$

Where β, θ^c, and θ^d are tabulated in Table 1. The fifth order scheme is adopted to reduce the dissipation. When a high order scheme is executed, a limiter function is usually used to suppress occurrence of numerical oscillations. However, to prevent the decay of the turbulent intensities of flow *the limiter function is then not adopted.*

The derivative terms of $A_{ij} = \frac{\partial u_j}{\partial x_i} + \frac{\partial u_i}{\partial x_j} - \frac{2}{3}(\nabla \bullet u)\delta_{ij}$ in Eq. (25) are computed by the fourth order central difference.

$$\frac{\partial u}{\partial x} = \frac{u_{i-2} - 8u_{i-1} + 8u_{i+1} - u_{i+2}}{12\Delta x} + o(\Delta x^4) \quad (32)$$

In order to compute the terms of $\overline{F}^k_1, \overline{F}^k_2$, and $\overline{F}^k_3$ of R^k shown in Eq. (12) in the curved linear coordinates (ξ, η, ζ), the $\overline{F}^k_1, \overline{F}^k_2$, and $\overline{F}^k_3$ can be expressed in terms of F_i indicated as follows, respectively.

$$\begin{aligned} \overline{F}^k_1 &= (\xi_{x_1}F_1 + \xi_{x_2}F_2 + \xi_{x_3}F_3)/J \\ \overline{F}^k_2 &= (\eta_{x_1}F_1 + \eta_{x_2}F_2 + \eta_{x_3}F_3)/J \\ \overline{F}^k_3 &= (\varsigma_{x_1}F_1 + \varsigma_{x_2}F_2 + \varsigma_{x_3}F_3)/J \end{aligned} \quad (33)$$

Then, $$R^k = -\left(\frac{3U^k - 4U^n + U^{n-1}}{2\Delta t}\right) - \{\delta_\xi[(\xi_{x_1}F_1 + \xi_{x_2}F_2 + \xi_{x_3}F_3)/J] + \delta_\eta[(\eta_{x_1}F_1 + \eta_{x_2}F_2 + \eta_{x_3}F_3)/J] + \delta_\zeta[(\varsigma_{x_1}F_1 + \varsigma_{x_2}F_2 + \varsigma_{x_3}F_3)/J]\}$$.

To substitute Eq. (33) into R^k of Eq. (20), Eq. (20) can be expressed as the following equation.

$$\begin{aligned} &L_{(i-1,j,k)}\Delta U^k_{p,(i-1,j,k)} + L_{(i,j-1,k)}\Delta U^k_{p,(i,j-1,k)} \\ &+ L_{(i,j,k-1)}\Delta U^k_{p,(i,j,k-1)} + D_{(i,j,k)}\Delta U^k_{p,(i,j,k)} \\ &+ U_{(i+1,j,k)}\Delta U^k_{p,(i+1,j,k)} + U_{(i,j+1,k)}\Delta U^k_{p,(i,j+1,k)} \\ &+ U_{(i,j,k+1)}\Delta U^k_{p,(i,j,k+1)} = \Gamma^{-1}R^k_{(i,j,k)} \end{aligned} \quad (34)$$

Table 1. Parameters used in Eqs. (30) and (31)

β	θ^c	θ^d	Order
1/3	0	0	3
1/3	−1/6	0	4
1/3	0	−1/6	4
1/3	−1/10	−1/15	5

Based on Yoon and Jameson [18] and modification, Eq. (20) can be expressed as follows.

$$(L+D)D^{-1}(D+U)\Delta\overline{U}_p^k = \Gamma^{-1}R^k \tag{35}$$

The solving procedures of Eq. (35) are briefly shown in the following processes.

1. To derive the following equations and execute a forward sweep process.

$$(L+D)\Delta U_p^* = \Gamma^{-1}R^k \tag{36}$$

Where $\Delta U_p^* = D^{-1}(D+U)\Delta\overline{U}_p^k$
To rearrange Eq. (36) as the following equations.

$$L\Delta U_p^* + D\Delta U_p^* = \Gamma^{-1}R^k \tag{37}$$

$$D\Delta U_p^* = \Gamma^{-1}R^k - L\Delta U_p^* \tag{38}$$

To obtain ΔU_p^* as follows.

$$\Delta U_p^* = D^{-1}(\Gamma^{-1}R^k - L\Delta U_p^*) \tag{39}$$

To expand Eq. (39) and execute a forward sweep process.

$$\begin{aligned}\Delta U^*_{p,(i,j,k)} = D_{(i,j,k)}[&\Gamma^{-1}R^k_{(i,j,k)} - L_{(i-1,j,k)}\Delta U^*_{p,(i-1,j,k)} \\ &- L_{(i,j-1,k)}\Delta U^*_{p,(i,j-1,k)} - L_{(i,j,k-1)}\Delta U^*_{p,(i,j,k-1)}]\end{aligned} \tag{40}$$

when $i=1$ or $j=1$ or $k=1$, the ΔU_p^* in RHS can be obtained from boundary conditions.

2. To derive the following equations and execute a backward sweep process.
To express ΔU_p^k in Eq. (36) as the following equation.

$$(D+U)\Delta\overline{U}_p^k = D\Delta U_p^* \tag{41}$$

To rearrange Eq. (41) as the following equation.

$$\Delta\overline{U}_p^k = \Delta U_p^* - D^{-1}U\Delta\overline{U}_p^k \tag{42}$$

To expand $\Delta\overline{U}_p^k$ and calculate the following equation.

$$\begin{aligned}\Delta U^k_{p,(i,j,k)} = \Delta U^*_{p,(i,j,k)} - D^{-1}_{(i,j,k)}[&U_{(i+1,j,k)}\Delta U^k_{p,(i+1,j,k)} \\ &+ U_{(i,j+1,k)}\Delta U^k_{p,(i,j+1,k)} + U_{(i,j,k+1)}\Delta U^k_{p,(i,j,k+1)}]\end{aligned} \tag{43}$$

At $i=nx$ or $j=ny$ or $k=nz$, to obtain the ΔU_p in RHS from boundary conditions.

3. To solve $\overline{U}_p^{k+1}$ as follows.

$$\overline{U}_p^{k+1} = \overline{U}_p^k + \Delta\overline{U}_p^k$$

4. To repeat steps 1–3 until $\frac{\overline{U}_p^{k+1} - \overline{U}_p^k}{\Delta\tau} \approx 0$ To use the condition of $\overline{U}_p^{n+1} = \overline{U}_p^{k+1}$, and obtain the next time step $\overline{U}_p^{n+1}$.

The advantages of usage of LUSGS implicit method are to improve efficiency and decrease artificial dissipation.

The isothermal and no slip conditions are adopted on the wall. The conditions are given as follows.

$$\begin{aligned} P(i,0,k) &= P(i,1,k) \\ u_1(i,0,k) &= -u_1(i,1,k) \\ u_2(i,0,k) &= -u_2(i,1,k) \\ u_3(i,0,k) &= -u_3(i,1,k) \\ T(i,0,k) &= 2T_h - T(i,1,k) \end{aligned} \tag{44}$$

Where T_h is wall temperature with a constant of $500\,k$. 0 indicates the ghost cell, and 1 indicates the cell most near the wall.

The computational domain used along the streamwise direction is periodical and the inlet and outlet conditions can be expressed as the following equations, respectively.

$$\begin{aligned} P(0,j,k) &= P(nx,j,k) \\ u_1(0,j,k) &= u_1(nx,j,k) \\ u_2(0,j,k) &= u_2(nx,j,k) \\ u_3(0,j,k) &= u_3(nx,j,k) \\ T(0,j,k) &= T(nx,j,k) \end{aligned} \tag{45}$$

$$\begin{aligned} P(nx+1,j,k) &= P(1,j,k) \\ u_1(nx+1,j,k) &= u_1(1,j,k) \\ u_2(nx+1,j,k) &= u_2(1,j,k) \\ u_3(nx+1,j,k) &= u_3(1,j,k) \\ T(nx+1,j,k) &= T(1,j,k) \end{aligned} \tag{46}$$

0 indicates the cell at the inlet, and $nx+1$ indicates the cell at the outlet.

The pressure gradient is the driving force to keep the continuous flow of channel. The local pressure gradient $\frac{\partial P(i,j,k)}{\partial x_1}$ includes two parts. One is the mean pressure gradient $\frac{\partial P_{mean}}{\partial x_1}$, which mainly drives the flow, and the other is the fluctuating pressure

gradient $\frac{\partial P_p}{\partial x_1}$ which, is a variable and induced by the turbulent flow. Then, it can be shown as follows.

$$\frac{\partial P}{\partial x_1} = \frac{\partial P_{mean}}{\partial x_1} + \frac{\partial P_p}{\partial x_1} = \mathrm{B} + \frac{\partial P_p}{\partial x_1} \tag{47}$$

The B is a source term in computing processes, and the periodic pressure conditions at the inlet and outlet are indicated as follows.

$$P_p(0,j,k) = P_p(nx,j,k) \tag{48}$$

$$P_p(nx+1,j,k) = P_p(1,j,k) \tag{49}$$

The mass flow rate in the channel flow is not easily kept conservative due to the viscous friction along the walls and the numerical dissipation. Therefore, Eq. (50) derived by Xu et. al [21]. is adopted to adjust the magnitude of B to keep the mass flow rate to be a constant during computation.

$$B^{n+1} = B^n - \frac{1}{\Delta t}\left[\left(\frac{\dot{m}}{A_C}\right)^0 - 2\left(\frac{\dot{m}}{A_C}\right)^n + \left(\frac{\dot{m}}{A_C}\right)^{n-1}\right] \tag{50}$$

Where A_C is the cross-flow area of channel, Δt is the physical time step, and $\dot{m}$ is the mass flow rate of the channel flow.

4. RESULTS AND DISCUSSION

In this work, air is the working fluid and the Prandtl number is 0.72. In order to validate the program, the turbulent channel flow resolved by the DNS method is performed at Reynolds number, based on the friction velocity of 940. Because of the wall effect, the dense grid distribution near the wall is needed and obtained by a curvilinear transformation, and the related equation proposed by [22] is shown in the following equation.

$$x_2 = h\frac{(2\alpha+\beta)\left(\frac{\beta+1}{\beta-1}\right)^{\frac{\eta-\alpha}{1-\alpha}} + 2\alpha - \beta}{(2\alpha+1)\left[1+\left(\frac{\beta+1}{\beta-1}\right)^{\frac{\eta-\alpha}{1-\alpha}}\right]} \tag{51}$$

In which, $\alpha = 0.5$ means the densities of grid distribution on both the top and bottom walls are equal. The more the magnitude of β is close to 1, the more the difference of the intervals of grids is remarkable and $\beta = 1.04$ is assigned. As a result, the smallest magnitude of interval Δx_2^+, which is the closest to the channel wall and equal to 1.5, is able to capture the turbulence scales as smaller as possible, and the largest magnitude of interval Δx_2^+ is located at the center and equal to 40. As for the other two directions of x_1 and x_3, the uniform grid distributions are selected and the magnitudes of the two intervals are $\Delta x_1^+ = 46.63$ and $\Delta x_3^+ = 23.32$, respectively. The figure of grid distribution

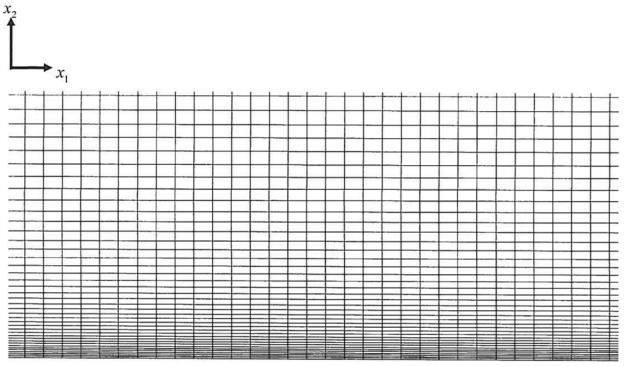

Figure 2. Grid distributions near the wall.

in x_1 and x_2 directions is shown in Figure 2, and the grid distribution in x_1, x_2, and x_3 directions are $160 \times 96 \times 64$. Besides, the initial conditions also influence the results of the turbulent flow apparently and should be taken into consideration carefully. In this study, the turbulent initial conditions are generated by a brilliant and practical method proposed by Klein et al. [23]. Figures 3 and 4 show the comparisons of the mean velocity profiles of $<u_1>$, and root-mean-square (r.m.s.) values of fluctuating velocities of $u'_{1,rms}, u'_{2,rms}$, and $u'_{3,rms}$ for $\varepsilon = 0.1$ with the benchmark solutions of the DNS data del Alamo et al. [24] obtained by spectral codes at $\mathrm{Re}_\tau = 940$ situation, respectively. The results are consistent so it can be inferred that $\varepsilon = 0.1$ is the optimal value. For lower Reynolds number, such as $\mathrm{Re}_\tau = 550$ and $\mathrm{Re}_\tau = 180$, the results of comparisons with

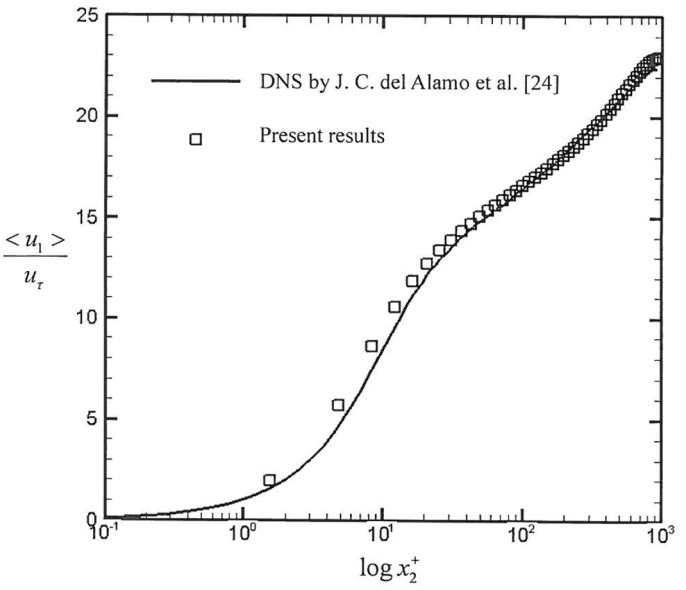

Figure 3. Comparison of mean velocities of u_1 [24] with present results for $\mathrm{Re}_\tau = 940$ ($\mathrm{Re} \cong 20000$).

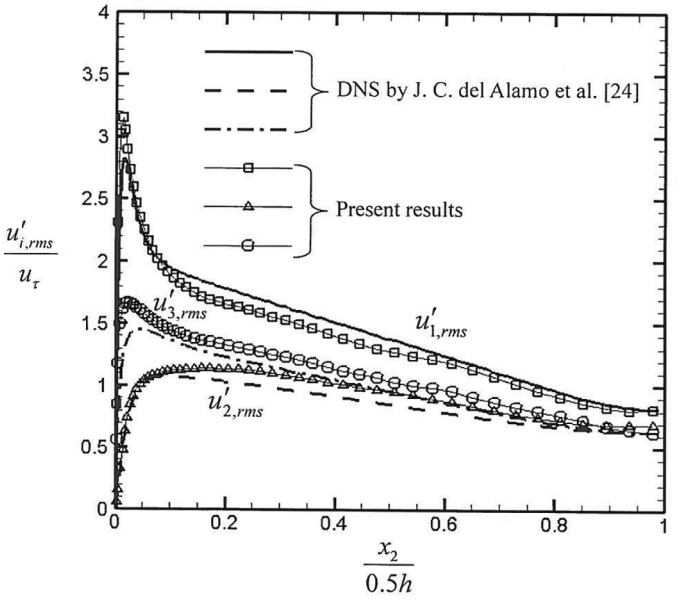

Figure 4. Comparisons of root-mean-square values of fluctuation velocities of $u'_{i,rms}$ [22] with present results for $Re_\tau = 940$.

the DNS data are still consistent for $\varepsilon = 0.1$. Due to the limitation of pages, the related results are not shown in the study. From the results mentioned above, it can be known that the Roe upwinding dissipation term can become an implicit turbulence model for LES as long as ε is set to 0.1. With the excellent advantages of easy implementation in the curvelinear coordinate and the validation from a low Reynolds number ($Re_\tau = 180$) to a high Reynolds number ($Re_\tau = 940$), this model can be used to study heat transfer mechanisms in the following.

The magnitudes of 180, 500, and 940 selected in this study are almost equivalent to the magnitudes of Reynolds number, of which the inlet velocity is regarded as the characteristic velocity of 2,700, 10,000, 20,000, respectively. The corresponding Mach numbers for these three cases are around 0.005, 0.014, and 0.026, respectively.

Phenomena shown in the following figures are at certain instants of fully developed turbulent flows. In Figure 5, temperature contours are indicated for situations of $Re_\tau = 180$, 500, and 940, respectively. In Figure 5*a*, a turbulent flow begins to be formed and the characteristics of turbulent flow are not remarkable. As a result, the temperature contour shown in Figure 5*a* of x_1x_3 plane, of which the distance (x_2^+) away from the bottom heat wall is 1.5, is almost uniform except several small regions. This phenomenon means the alternate mixture of different temperature layers to be slight. On x_1x_2 and x_2x_3 planes, the magnitudes of temperature distribution from the bottom heat wall to the upper region gradually decrease, and phenomena of alternate mixture of different temperature layers near the wall region are scarcely found because of the weakness of fluctuating velocity in x_2 direction.

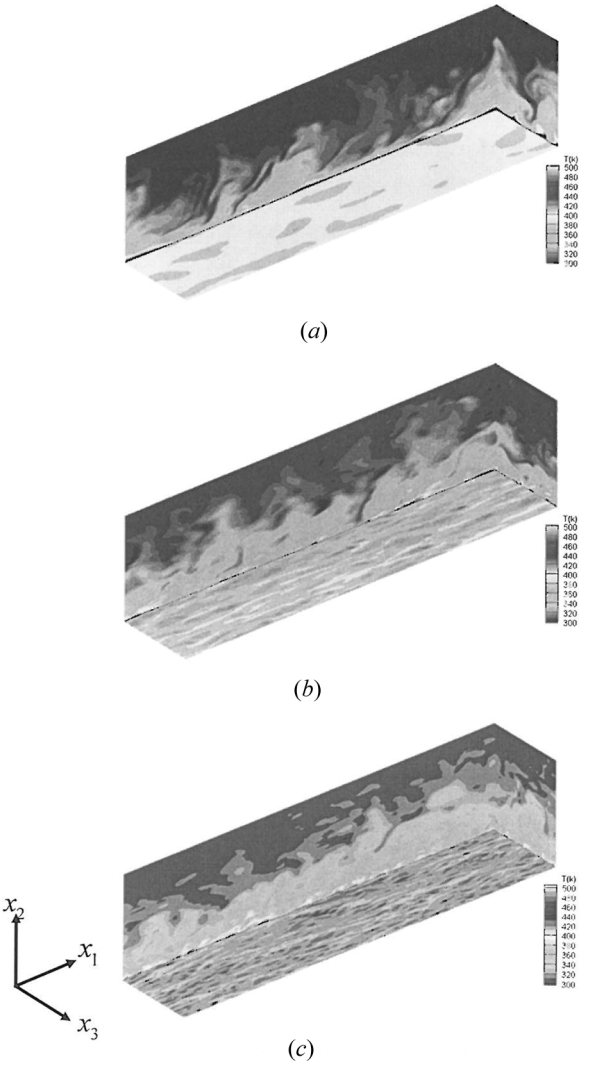

Figure 5. Temperature contours on x_1x_2, x_1x_3 and x_2x_3 planes under different magnitudes of Re_τ of *a*) 180 ($\mathrm{Re} \cong 2700$), *b*) 500 ($\mathrm{Re} \cong 10000$), and *c*) 940 ($\mathrm{Re} \cong 20000$).

In Figure 5*b*, the magnitude of Re_τ is increased to 500, and the behaviors of characteristics of turbulent flow naturally become apparent. Motions of alternate mixture of different temperature layers are drastic because fluctuation velocities in each direction become large. As a result, the presence of fluids having different temperatures is remarkably indicated on the horizontal plane of $x_1x_3(x_2^+ = 1.5)$. On the vertical planes of x_1x_2 and x_2x_3, accompanying characteristic motions of ejection and swept of turbulent flow, fluids possessing different temperatures move up and down drastically near the wall region; therein, the possibility of cooling fluids directly impinging on the bottom heat wall increases. This is the main reason for the heat transfer rate of turbulent flow being superior.

In Figure 5*c*, the magnitude of Re_τ is equal to 940. Certainly, the behaviors of turbulent flow become more apparent than those of the two previous situations. Then, on the x_1x_3 plane, streaks of light color interlace along the x_1 direction to be observed, and spots of dark color are irregularly distributed. This phenomenon indicates the occurrence of drastic alternate mixture of different temperature layers near the wall region. On the planes of x_1x_2 and x_2x_3, the temperature layer near the wall region is irregularly invaded by fluids possessing different temperatures, the complete temperature layer near the wall similar to that of Figure 5*a* no longer exists.

In Figure 6, different isothermal surfaces of fluids in the space near the wall under different magnitudes of Re_τ of 180, 500, and 940 are indicated, respectively. Due to the indication of the three-dimensional geometry shown in the figures,

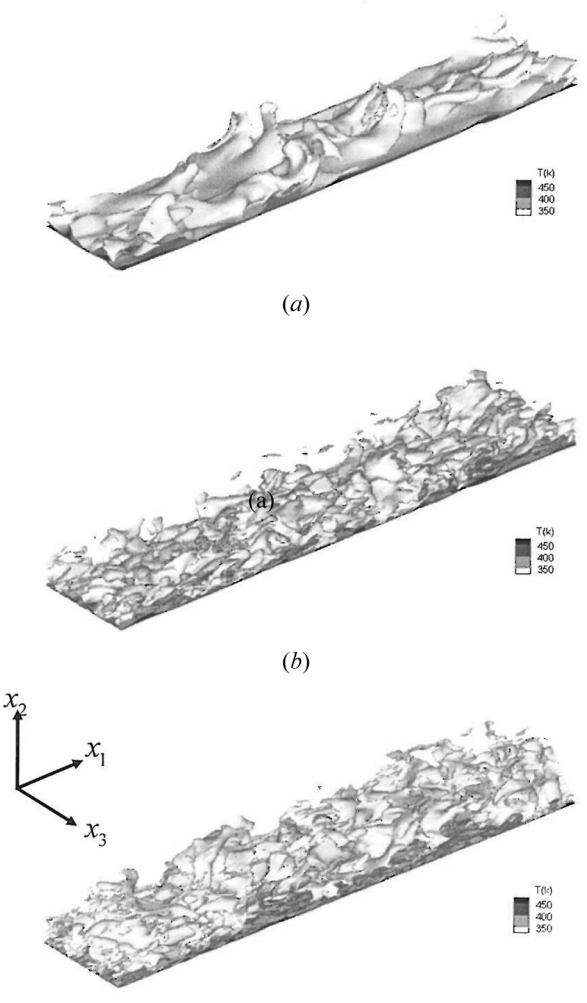

Figure 6. Isothermal surfaces of fluids for $Re_\tau = a)$ 180, *b*) 500, and *c*) 940 situations.

outward appearances of isothermal surfaces of fluids are observed from a certain visual angle. In Figure 6*a*, the initial stage of turbulent flow is formed, and the characteristic behaviors of turbulent flow are not apparent. The fluctuation velocity is weak that causes a cluster of big lumps of fluids possessing different isothermal surfaces to be observed. Accompanying the increment of magnitude of Re_τ, the characteristic behaviors of turbulent flow become remarkable. The fluctuating velocities are enlarged in each direction that results in a cluster of big lumps of fluids mentioned above being torn into an aggregation of small fragments of fluids possessing different isothermal surfaces, shown in Figures 6*b* and 6*c*, respectively.

In Figure 7, density contours in three different planes of x_1x_2, x_1x_3, and x_2x_3 are shown, respectively, for the $\mathrm{Re}_\tau = 940$ situation. The contour of density shown in the x_1x_3 plane is very close to the bottom heat wall and $x_2^+ = 1.5$. Because of the consideration of compressibility of fluid, the density of fluid becomes a variable. The darker the color is, the lighter the density is indicated. Then, most regions of this plane filled with fluids of light density are observed. However, a few slightly bright regions composed of fluids having slightly heavy density irregularly mixing in dark regions are founded out. This phenomenon is mainly caused by the fluctuation velocity in the x_2 direction. This characteristic phenomenon certainly appears in the boundary layer of turbulent flow. Similar phenomena are observed in planes of x_1x_2 and x_2x_3. Part of the fluids of light density distributed in the bottom region of the thermal boundary layer irregularly flee up to the upper region, and the density becomes heavy, gradually, because of it accompanying the decrement of temperature in the x_2 direction. Meanwhile part of the fluids which are located at slightly upper regions away from the heated bottom surface possess a relatively heavy density rapidly implemented in the space vacated by the escape of the fluids of light density mentioned above. As a result, an irregular distribution of densities is indicated in the whole near wall region.

In Figure 8, local instantaneous Nusselt numbers on the central cross-section of the x_1x_3 plane and average Nusselt numbers of the x_1x_3 plane of three situations

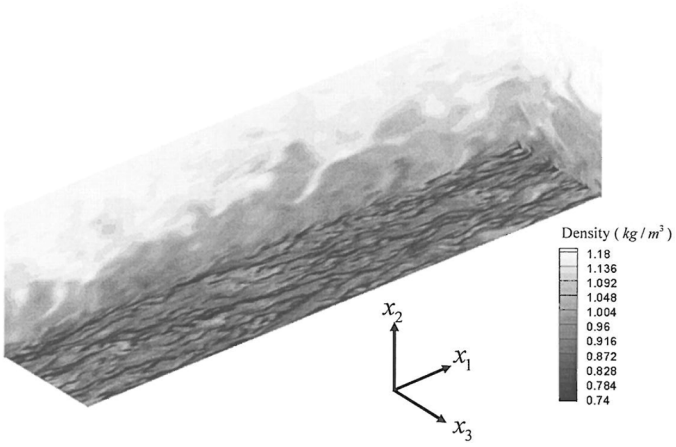

Figure 7. Density contour ($\mathrm{Re}_\tau = 940$).

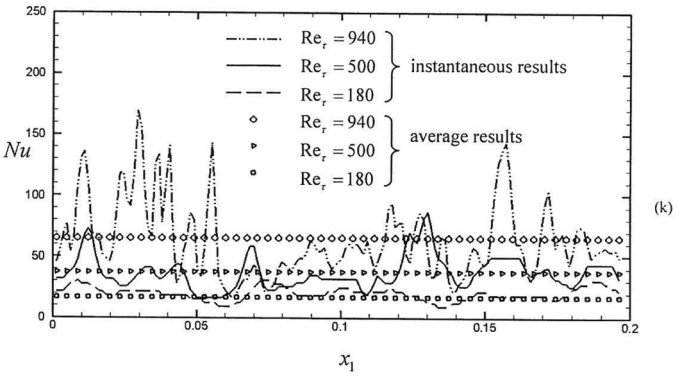

Figure 8. Local instantaneous Nusselt number distributions on the wall along the central cross-section of the x_1x_3 plane and average Nusselt numbers on the x_1x_3 plane.

are indicated, respectively. The local instantaneous Nusselt number Nu and average Nusselt number $\overline{\mathrm{Nu}}$ are defined as follows, respectively.

$$\mathrm{Nu} = \frac{l_2}{k_0(T_h - T_c)}\left[k(T)\frac{\partial T}{\partial x_2}\right]_{wall} \tag{52}$$

$$\overline{\mathrm{Nu}} = \frac{1}{A}\int\int \frac{l_2}{k_0(T_h - T_c)}\left[k(T)\frac{\partial T}{\partial x_2}\right]_{wall} dx_1 dx_3 \tag{53}$$

Where A is the area of the heat surface.

The larger the magnitude of Re_τ is, the magnitudes of the main stream and fluctuating velocities are faster. As a result, accompanying with the increment of

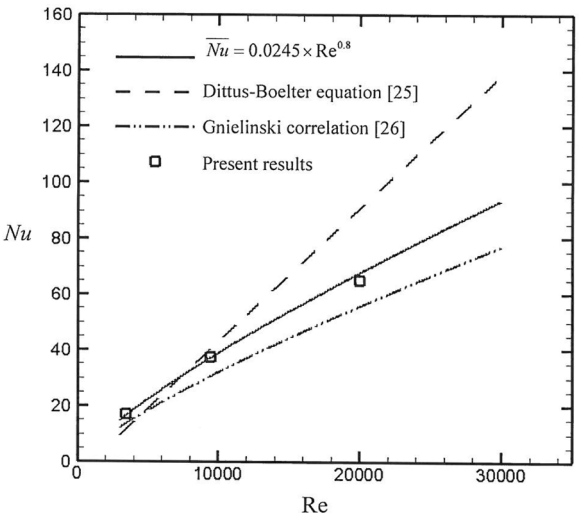

Figure 9. Comparison of present results with existing results.

Re_τ, the magnitude of the average Nusselt number becomes larger and the variation of local instantaneous Nusselt number becomes drastic. In terms of practical applications, it also means that the possibility of the unexpected failure, such as a thermal shock at the high Reynolds number, is much higher than that at the low Reynolds number.

The average Nusselt number obtained from this study can be expressed as a function of the Reynolds number, which is based on the average flow velocity and the height of channel, and shown in the following equation.

$$\overline{\mathrm{Nu}} = 0.0245 \times \mathrm{Re}^{0.8}. \tag{54}$$

The relationship between the average Nusselt number and Reynolds number presents an exponential form. Figure 9 shows that the trend of Eq. (54) is similar to the Dittus-Boelter correlation [25] for smooth tubes and the Gnielinski equation [26] is tailored to forced convection in a turbulent pipe flow.

5. CONCLUSION

A numerical study of compressible turbulent forced convection in a channel flow is performed. Several conclusions are summarized as follows.

1. An implicit turbulence model for LES is developed to investigate heat transfer rates of a three-dimensional channel. An appropriately empirical formula can be derived.
2. The increment of Reynolds number causes the strength of the Reynolds stress to be stronger that leads to a cluster of big lumps, composing different isothermal surfaces of fluids, and are gradually torn into an aggregation of fragments of different isotheral surfaces of fluids.
3. Variations of instantaneous local Nusselt numbers are very drastic under high Reynolds number situations. This phenomenon should be avoided in order to get rid of the heat damage caused by thermal shock.
4. With the excellent advantages of easy implementation, the numerical method developed in this study is promising for turbulence simulation in the future.

REFERENCES

1. W. R. Briley, H. McDonald, and S. J. Shamroth, At Low Mach Number Euler Formulation, and Application to Time Iterative LBI Schemes, *AIAA*, vol. 21, no. 10, pp. 1467–1469, 1983.
2. E. Turkel, Preconditioned Methods for Solving the Incompressible and Low Speed Compressible Equations, *J. Comput. Phys.*, vol. 72, pp. 277–298, 1987.
3. D. Choi and C. L. Merkel, Application of Time-Iterative Schemes to Incompressible Flow, *AIAA*, vol. 25, no. 6, pp. 1518–1524, 1985.
4. D. Choi and C. L. Merkel, The Application of Preconditioning in Viscous Flows, *J. Comput. Phys.*, vol. 105, pp. 207–223, 1993.
5. P. L. Roe, Approximation Riemann Solver, Parameter Vectors, and Difference Schemes, *J. Comput. Phys.*, vol. 43, pp. 357–372, 1981.

6. J. M. Weiss and W. A. Smith, Preconditioning Applied to Variable, and Constants Density Flows, *AIAA*, vol. 33, pp. 2050–2056, 1995.
7. B. J. R. Thornbe and D. Drikakis, Numerical Dissipation of Upwind Schemes in Low Mach Flow, *Int. J. Numer. Meth. Fluids*, vol. 56, pp. 1535–1541, 2008.
8. S. Dellacherie, Analysis of Godunov Type Schemes Applied to the Compressible Euler System at Low Mach Number, *J. Comput. Phys.*, vol. 229, pp. 978–1016, 2010.
9. B. Lessani, J. Ramboer, and C. Lacor, Efficient Large-Eddy Simulations of Low Mach Number Flows using Preconditioning, and Multigrid, *J. Comput. Phys.*, vol. 18, pp. 221–233, 2002.
10. X. Xiaofeng, J. S. Lee, and R. H. Pletcher, A Compressible Finite Volume Formulation for Large Eddy Simulation of Turbulent Pipe Flows at Low Mach Number in Cartesian Coordinates, *J. Comput. Phys.*, vol. 203, pp. 22–48, 2005.
11. N. Alkishriwi, M. Meinke, and W. Schroder, A Large-Eddy Simulation Method for Low Mach Number Flows using Precondition, and Multigrid, *Computers & Fluids*, vol. 35, pp. 1126–1136, 2005.
12. J. A. Domaradzki and N. A. Adams, Direct Modeling of Subgrid Scales of Turbulence in Large Eddy Simulations, *J. of Turbulence*, vol. 3, pp. 1–19, 2002.
13. J. A. Domaradzki, K. C. Loh, and P. Y. Patrick, Large Eddy Simulations using the Subgrid-Scale Estimation Model, and Truncated Navier-Stokes Dynamics, *Theor. Comput. Fluid Dyn.*, vol. 15, pp. 421–450, 2002.
14. S. Stolz and N. A. Adam, An Approximate Deconvolution Procedure for Large-Eddy Simulation, *Phys. Fluids*, vol. 11, pp. 1699–1701, 1999.
15. C. Fureby and F. F. Grinstein, Monotonically Integrated Large Eddy Simulation of Free Shear Flows, *AIAA*, vol. 37, pp. 544–556, 1999.
16. J. A. Domaradzki and S. Radhakrishnan, Effective Eddy Viscosities in Implicit Modeling of Decaying High Reynolds Number Turbulence with and without Rotation, *Fluid Dyn. Res.*, vol. 36, pp. 385–406, 2005.
17. T. Tankitul and J. A. Domaradzki, Large Eddy Simulations using Truncated Navier-Stokes Equations with the Automatic Filtering Criterion, *J. of Turbulence*, vol. 11, pp. 1468–5248, 2010.
18. S. Yoon and S. Jameson, Lower-Upper Symmetric-Gauss-Seidel Method for the Euler and Navier-Stokes Equations, *AIAA*, vol. 26, pp. 1025–1026, 1988.
19. T. B. Tong, A Parallel Finite-Volume Algorithm for Large-Eddy Simulation of Turbulence Flows, *Computers & Fluids*, vol. 29, pp. 877–915, 2000.
20. I. Abalakin, A. Dervieux, and T. Kozubskaya, A Vertex Centered High Order MUSCL Scheme Applying to Linearized Euler Acoustics, *INRIA*, no. 4459, 2002.
21. X. F. Xu, J. S. Lee, and R. H. Pletcher, A Compressible Finite Volume Formulation for Large Eddy Simulation of Turbulent Pipe Flows at Low Mach Number in Cartesian Coordinates, *J. Comput. Phys.*, vol. 203, pp. 22–48, 2005.
22. K. A. Hoffmann and S. T. Chiang, *Computational Fluid Dynamics for Engineers*, Engineering Education System, Wichita, Kansas, 1993.
23. M. Klein, A. Sadiki, and J. Janicka, A Digital Filter Based Generation of Inflow Data for Spatially Developing Direct Numerical or Large Eddy Simulation, *J. Comput. Phys.*, vol. 186, pp. 652–665, 2003.
24. J. C. del Alamo, J. Jimenez, P. Zandonade, and R. D. Moser, Scaling of the Energy Spectra of Turbulent Channels, *J. Fluid Mech.*, vol. 500, pp. 135–144, 2004.
25. P. I. Frank, P. D. David, L. B. Theodore, and S. L. Adrienne, *Fundamentals of Heat and Mass Transfer*, 6th ed., pp. 490–515, 2006.
26. P. I. Frank and P. D. David, *Fundamentals of Heat and Mass Transfer*, 4th ed., p. 493, 1996.